Optimizing Motor Performance with Improved Fractional Order Darwinian Particle Swarm Optimization and Fuzzy Logic Controllers: A Comparative Study in Torque Control

M Mohamed Ajmal Mahasin[1], R Sanjay[1], D Rathinavel[1], E Raviprakash[1], V Vinubalan[1]*

[1]Department of Mechanical Engineering, Nandha Engineering College, Perundurai 638 052, Tamilnadu, India

Abstract: Utilizing fuzzy logic controllers (FLCs) and the improved fractional ordered Darwinian particle swarm optimization method (IFODPSO), this paper demonstrates a way to boost motor performance. The system is able to generate torque instantly and respond quickly because it uses direct torque control (DTC) approaches that are regulated by IFODPSO. Motor performance improvement with IFODPSO and fuzzy logic controllers is the motive of this study. The regulation of torque in motor applications is the particular issue that is being tackled. The research compares the IFODPSO-FLC method's performance with that of typical field-oriented control (FOC) method and DTC method. In contrasted with more conventional FOC and DTC methods, the results obtained by the IFODPSO-FLC methodology show promise for torque control, highlighting the significance of the findings. To further enhance system efficiency at low speeds, the suggested PI-fuzzy opposition estimation accounts for fluctuations in stator resistance. An innovative and effective strategy is the integration of fractional-order FLCs with Darwinian particle swarm optimization (DPSO). The outcomes are assessed with the use of MATLAB-Simulink and the performance that is derived from them shows promise for effective motor control applications.

1 Introduction

The usage of electric motors, which provide numerous benefits in relation to adaptable traction stability, is a key distinction between electric vehicles (EVs) and traditional cars driven by internal combustion engines [1]. Since electric motors are better at controlling torque than internal combustion engine vehicles (ICEVs), electric vehicles will reach previously unimagined levels of safety in near future [2]. Note that well-controlled electric motors have a few noticeable benefits, such as the responsiveness of nonlinear processes and easy-to-implement dispersion-in-wheel motor systems. These benefits extend to the generation of energy through traction, braking, and simple torque feedback [3]. According to the published research, these systems primarily serve to: To maintain the vehicle's stability and provide superior braking performance, antilock braking systems (ABS) prevent the wheels from locking up when using the brakes [4]. To keep tyres from slipping when taking off or accelerating, traction control (TC) is used. Additionally, TC is referred to as "acceleration slip regulation" in technical publications [5, 6]. There are numerous methods for controlling the induction motor torque. Direct torque regulation and FOC are becoming more popular due to their adherence to energy-while-speed standards that are not affected by changes in the load factor [7]. Blaschke created vector control in 1970 and released it to the public in 1971; it is a field-focused control system. The vectors of voltage, current, and magnetic flux were controlled using this method. The technology's flux and torque components are also detachable, just as those of an independently stimulated direct current (DC) motor [8]. The potential for simulated control of high-speed induction motor speeds. The technology employed in the simulation was in DC. The system was tested using the fuzzy-PID model in both loaded and unloaded scenarios. Energy consumption is 4.5% higher in the no-load test compared to the existing method according to the suggested technique [9]. Fuzzy PID uses 1.03% less power than traditional PID when tested under load situations. In recent years, numerous nonlinear control methods have been employed in the study of wheel slip control. To address nonlinear adhesion issues caused by nature and wheel slip, a model control structure known as a behaviour model control (BMC) is described [10]. This structure is well-suited to nonlinear systems and applies control to them. Thus, the skids disappeared, guaranteeing that the car would remain stable. Hybrid electric vehicles that use in-wheel motors and a fuzzy logic (FL) slip control system were suggested. Researchers presented a FL-based antiskid control structure to focus the primary problem with powertrain systems [11]. The vehicle will remain stable in all weather conditions due to this design. Develop a controller for controlling wheel slip using a sliding mode framework examines the relationship between a nonlinear predictive model and acceleration slip

* Corresponding Author: mohamed.ajmal@nandhaengg.org

regulation (ASR) control, a controller used in electric cars equipped with four-wheel motors. A potential instability of the vehicle could occur if one of the four wheels loses adhesion [12]. Switching to traction or braking mode will fix this issue. Maintaining control of the slip ratios is crucial for electric vehicle safety and dynamic performance, preventing wheel locks and slides during acceleration and braking. A novel longitudinal electrical system was developed for EVs including 4 PMS in-wheel motors, changing ABS and ASR. By dynamically regulating the in-wheel PMS motor torque, it is also possible to achieve good acceleration performance [13,14]. Since electric automobiles were introduced, the number of individuals using them has climbed substantially. In Figure 1(a), shows an example of a conventional electric vehicle that uses a concentrated power system, meaning that it has just one motor and a differential to turn the wheels in both directions. Basically, electric vehicles are just regular cars that use motors and batteries instead of engines, as opposed to the more common internal combustion engines. This means that EVs may have less effective motion control systems, more maintenance needs, and more mechanical components.

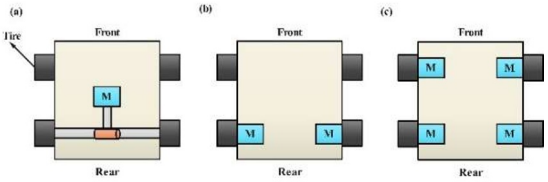

Fig. 1. (a) Front wheel and back wheel, (b) motor of back wheel, (c) 4 wheels, (d) in-wheel motor

Fig. 1(b) shows that EVs can be developed more efficiently with the introduction of novel topologies made possible by in-wheel motor technology. Throughout the next hundred years, in-wheel motor technology underwent consistent advancements. Power electronics and electromagnetic technology have come a long way in the last few decades, which has led to significant improvements in in-wheel motors. Figures 1(c) and 1(d) shows the in-wheel motor layout, which has numerous advantages over the conventional electric vehicle design. In this setup, the motor is located in the middle and uses axes to drive either two or four wheels.

Vehicles equipped with all-wheel drive exhibit exceptional control.

Extremely low energy consumption.

The power train topologies are a reasonable option for electric vehicles due to the benefits of in-wheel motors. Electricity is the driving force behind an electric vehicle. The powertrains of the next generation of electric vehicles are entirely powered by electricity. This part consists of wheels, a gearbox, and a motor drive. Historically, DC motors have been utilized in electric propulsion due to their traction appropriateness and ease of speed control [15]. As a possible alternative for electric vehicle traction at varied speeds, permanent magnet synchronous motors (PMSM) have lately been the subject of extensive research. Electric vehicles are far better for the environment than cars driven by internal combustion engines [16]. The electric vehicle's power distribution networks are an additional perk, on top of the vehicle's low environmental impact and high energy efficiency. Electric vehicle (EV) battery packs have a number of issues, including a lengthy charging time and inefficiency. Electric vehicles rely heavily on efficient energy management systems; other essential factors include the best possible motor design, the right choice of drive, and the most effective method of control. Propeller systems (motors) used in electric vehicles should be able to generate large amounts of torque (300–400 %), accelerate quickly, produce little noise, require little in the way of maintenance, be compact, light, and inexpensive. An insensitive motor to the acceleration forces is essential for the efficient operation of an electric vehicle. There are squirrel-cage induction motors that include most of the features listed above [17]. The flux reference is always determined by the motor speed, regardless of the operating conditions. During steady-state (constant speed) operation, efficiency optimum management is required due to the limited energy of the battery. Detecting rotor resistance is essential for optimal rotor control at steady-state. In order to conduct DTC, exact measurements of stator resistance are required. A thermal sensor's value is dependent on temperature. To summarize the work, the following factors were considered: To maximize motor performance, a FLC is integrated with improved fractional ordered DPSO. In order to improve efficiency at low speeds, the PI-fuzzy opposition estimate method takes stator resistance changes into consideration. Both the pollution rate generated by emissions produced from internal combustion engines and the planet's depleting oil reserves are concerning in today's world [18, 19]. Vehicle technology that runs on electric power, that considered a clean energy source, could be the solution. The numerous advantages of electric vehicles over conventional cars driven by internal combustion engines make them a serious contender in the market for replacement vehicles [20]. Currently, electric vehicles rely on batteries for their electricity, but many different energy storage technologies are being researched at the same time. To be effective, batteries need to be able to hold a lot of power, drain a lot of current, charge empty cells when positive braking is applied, and last for a long time [21, 22]. Industrial users, including electric car manufacturers like traction systems that use induction motors. Cities can build a transportation system which is clean, efficient, and enjoyable because of electric motors. Induction motors provide efficient performance when operated under steady-state conditions and with rated loads [23]. In order to achieve the best possible transient response, a variable speed motor is usually driven at flux rated using a variable frequency motor. In the past, several various methods were proposed to enhance an induction motor's efficiency, particularly when working under low load conditions. In order to attain the maximum level of efficiency, some aspects need to be considered. The second method, known as the "search controller," is feedback-based and looks for the most efficient solution by employing a search strategy. Although field-oriented control offers excellent

dynamic and stationary performance for induction drives, it frequently disregards the minimization of loss. Therefore, combining FOC with LMC can result in energy savings. The use of coordinate transformation, FOC necessitates a very precise knowledge of the machine model's characteristics and involves a substantial amount of labour in terms of cost [24]. DTC is a visual look-up device that controls the stator flux and synchronized electromagnetic energy of the machine. Consequently, fault-tolerant control (FTC) systems have been the focus of a great deal of research. To improve residual capabilities in the event of a phase-loss defect, multiphase PM machines are typically employed [25, 26]. To further decouple the motor phases, it is possible to accomplish magnetic separation using fractional-slot concentrated windings (FSCW). In addition to improving fault tolerance, the FSCW may produce parallel magnetic motive forces and back-electro motive forces through the use of specific high-harmonic components. The five-stage fault-tolerant FSCW interior permanent magnet motor is proposed in this study to solve the problems described before [27]. Because of its wide speed spectrum, high dependability, and fault tolerance, this FTFSCWIPM motor is well-suited for use in electric cars. It is common practice for AC drives with maximum performance to employ both DTC and FOC. For EV applications that demand top performance, a DTC is the way to go because it has many advantages over FOC, such as a simple design, decreased dependency on parameters, and fast torque response [28, 29]. Some research on DTC approaches that multiphase motors that operate in a healthy environment have been conducted. A better DTC method was considered by the researchers for the minimum-speed operation of the five-phase induction motor.

2 Proposed Method

2.1 The Electric Vehicle Analyzed Structure

Using PMS in wheel motors, an independent inverter is shown in Figure 2(a). According to Figure 2(b), the two pairs of in-wheel bi-PMS motors will be supplied by a single inverter on each side, with two simultaneous connections. The control issues related to these systems have been researched. Since the second structure can be built using an electric differential system, it will be our primary focus. The usage of autonomously controlled electric motors was lead to two additional benefits: (i) enhanced driving comfort and (ii) a decrease or elimination of the need for friction brakes for recovering braking energy and controlling wheel slide.

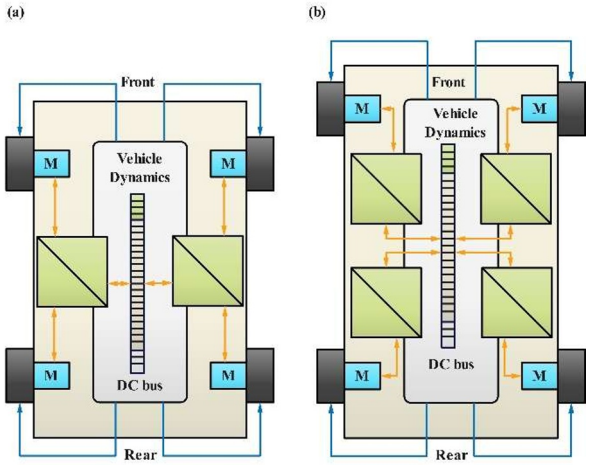

Fig. 2. Electric Vehicles (a) 2 inverters and (b) 4 inverters

2.2 Dynamic Model

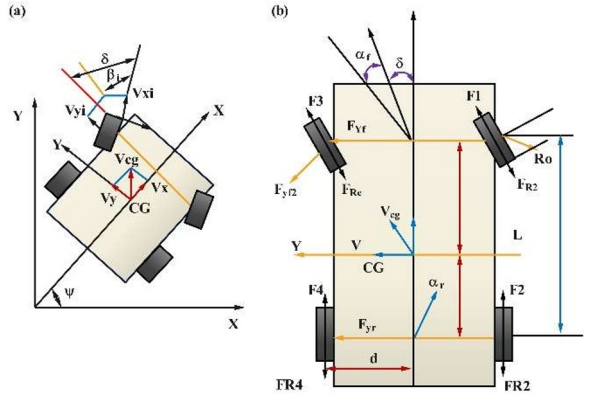

Fig. 3. Vehicle model

An automobile's dynamic model can be defined using three equations: one equation for each of the 3 translational motions and yet another for yaw-directed rotating motion, as shown in Figure 3.

$$M_v\ddot{X} = F_x \quad (1)$$

$$M_v\ddot{Y} = F_y \quad (2)$$

$$J_v\ddot{\Psi} = M_z \quad (3)$$

The values of xv for longitudinal velocity, yv for lateral velocity, &,Ψ yaw for rotational rate and Jv for moment of inertia are presented. The total energies acting on the X, Y, and Z planes for the entire yawing moment are denoted by Fx, Fy and Mz, respectively. They are related to the reference frame velocities in the following way:

$$\begin{bmatrix}\dot{X}\\ \dot{Y}\\ \dot{\Psi}\end{bmatrix} = \begin{bmatrix}\cos(\Psi) & -\sin(\Psi) & 0\\ \sin(\Psi) & \cos(\Psi) & 0\\ 0 & 0 & 1\end{bmatrix}\begin{bmatrix}v_x\\ v_y\\ r\end{bmatrix} \quad (4)$$

A mathematical model can be obtained in various ways; in this case, Lagrange equations will be employed [30]. The kinetic energy of the vehicle, disregarding the interaction with tire weight, can be stated as follows:

$$t = \frac{1}{2}M_v(\dot{X}^2 + \dot{Y}^2) + \frac{1}{2}J_v\dot{\Psi}^2 \quad (5)$$

The equations of motion can be derived from this relationship:

$$\frac{d}{dt}\left(\frac{\partial t}{\partial qi}\right) - \frac{\partial t}{\partial qi} = Q_i \quad (6)$$

The coordinates X, Y, and M for Qi indicate the corresponding services F (x, y) and Mz. The following result is obtained by considering the vehicle frame along with the required time derivatives and forces Fx and Fy:

$$F_x = M_v(\dot{v}_x - rv_y) \quad (7)$$

$$F_y = M_v(\dot{v}_y - rv_y) \quad (8)$$

$$M_z = J_v\dot{r} \quad (9)$$

The cornering forces are determined by the cornering stiffness and the sideslip angle (f and r), according to a linear tyre model (Cf, and Cr).

$$F_{xf} = -C_f\alpha_f \quad (10)$$

$$F_{yr} = -C_r\alpha_r \quad (11)$$

With the use of the steering, angular, longitudinal, and lateral angles, we can find the wheel swing angle. Equation (12) expresses the sideslip angles explicitly with respect to the front and rear axles.

$$\alpha_f = \tan^{-1}\left[\frac{v_y + l_f r}{v_x}\right] - \delta \quad (12)$$

$$\alpha_r = \tan^{-1}\left[\frac{v_y - l_f r}{v_x}\right] \quad (13)$$

The three basic equations of motion can be derived by first determining the effect of x, y, and z forces on a vehicle, then finding the varying moments related to spinning around its own centre of gravity (CG), and lastly substituting the equations obtained from the previous step (Eq. (14)) into the original equation (Eq (16).

$$\dot{v}_x = v_y r + \frac{F_{t1}+F_{t2}+F_{t3}+F_{t4}-F_{\text{rers}}}{M_v} + \frac{C_f\delta}{M_v}\left[\frac{v_y + rl_r}{v_x} - \delta\right] \quad (14)$$

$$v_y = \left[-\frac{C_r + C_f}{M_v v_x}\right]v_y + \left[-\frac{C_r l_r + C_f l_f}{M_v v_x} - v_x\right]r + \frac{C_f}{M_v}\delta \quad (15)$$

$$\dot{r} = \left[\frac{C_r l_r - C_f l_f}{J_v v_x}\right]v_y - \left[\frac{C_r l_r^2 + C_f l_f^2}{J_v v}\right]r + \frac{C_f l_f}{J_v}\delta + \frac{d}{J_v}(F_{t1} + F_{t2} - F_{t3} - F_{t4}) \quad (16)$$

Taking the vehicle strategy into account, (a) the model under stringent conditions; (b) the aerodynamic drag forces for directions F, roll force F_R, with climb force F_C; and (c) the motor-generated tractive forces, $Ft1$, $Ft2$, $Ft3$ and $Ft4$. Here are the expressions:

$$F_x = M_v(\dot{v}_x - rv_y) \quad (17)$$

$$F_y = M_v(\dot{v}_y - rv_y) \quad (18)$$

$$M_z = J_v\mathrm{r} \quad (19)$$

The wheel side slip (r and f) angle is determined by the force supplied to a tyre following a specific slip, which is the longitudinal component that an engine driver determines. Another approach to define the longitudinal sliding for each wheel is as follows:

$$\lambda_x = \frac{R_w w_x - u_{tx}}{\max(R_w w_x, u_{tx})}, x \in (1, \dots, 4) \quad (20)$$

Here are the traction forces among the tyre and the ground, as described by Pacejka's magical model:

$$\mu = c_1\left[\sin\left[c_2\tan^{-1}\left[c_3\lambda - c_4\left[c_3\lambda - \tan^{-1}[c_3\lambda]\right]\right]\right]\right] \quad (21)$$

The sets of coefficients for $c1$, $c2$, $c3$ and $c4$ are shown in Table 1.

The longitudinal force generated by the four wheel-mounted motors can be calculated using the following formula.

$$F_{tx} = \frac{gM_v}{4}\mu_x\cos\left[\alpha_p\right], x\epsilon(1, \dots, 4) \quad (22)$$

Table 1. The friction concept's parameters.

Surface	c_1	c_2	c_3	c_4
Normal	1	1,10	11	0,98
Snow	0,4	3	6	2
Wet	0,84	3,4	13	2
Ice	0,2	3	5	2

2.3 Field-Orientation Control

The FOC uses an orthogonal transformation, changing the a-b-c coordinates to dq0 coordinates, due to the decoupling of torque and flux components. In transient situations, the response time of torque controller can be reduced by regulating the PI controllers output voltage. The components include a voltage source inverter (VSI) and either an induction motor controller, a pulse width modulation (PWM), or an integrated gate bipolar transistor (IGBT) block for current control. In this comparison, the PI controller was used to estimate the speed variation and a rotor velocity (r) is evaluated contrasted with the standard speed (r). The quantity of energy generated by the benchmark torque is limited by a PI controller limiter (Tk). The components of the current axes in quadrature and DC are combined to form references currents in three phases. A comparison is made between the reference winding frequency ranges and the measured winding current, and the PWM block receives the error information. A switching signal is built and utilized using these Eqs. (23)-(29).

$$x_{ds} = \left[\Psi_{ds} - \frac{L_m}{L_r}\Psi_{dr}\right]\frac{1}{\sigma L_s} \quad (23)$$

$$x_{qs} = \left[\Psi_{qs} - \frac{L_m}{L_r}\Psi_{qr}\right]\frac{1}{\sigma L_s} \quad (24)$$

$$x_{dr} = \left[\Psi_{dr} - \frac{L_m}{L_s}\Psi_{ds}\right]\frac{1}{\sigma L_r} \quad (25)$$

$$x_{qr} = \left[\Psi_{qr} - \frac{L_m}{L_s}\Psi_{qr}\right]\frac{1}{\sigma L_r} \quad (26)$$

Here $\sigma = 1 = -\frac{L_m^2}{L_r L_s}$

$$t_e = \frac{3}{2}\left[\frac{P}{2}\right]\left[\Psi_{dr}x_{qs} - \Psi_{qr}x_{ds}\right] \quad (27)$$

$$\Psi_r = \sqrt{\Psi_{dr}^2 + \Psi_{qr}^2} \quad (28)$$

Mechanical power can be generated using three-phase induction motors by means of three-phase electrical energy. The stator generates a magnetic field when it receives alternating current (AC) electricity. Alternatively, synchronous motors spin the rotor by use of an applied magnetic field. The secondary winding,

which is created by the rotation of the rotor winding, is used to power the transformer.

2.4 Direct Torque Control

IGBTs form the basis of the inverter, which comprises a torque controller and a speed controller that incorporates motion with DTC. If the rotor speed is determined using the standard speed leads, an incorrect signal was produced. To maintain control of the torque, a torque limiter is employed. Table 1 shows the relationship between the torque in actual units and a limited torque reference (Tref) calculated by a machine, which allows one to calculate torque inaccuracy. A reference speed of motor is found by the stator flux and the projected rotor speed flux. The VSI's switching vectors are determined by flux and torque errors. Thus, the amount of torque is determined by the stator and rotor energies:

$$t_e = \frac{3}{2}\left[\frac{P}{2}\right]\frac{L_m}{LL'}|\Psi_r||\Psi_s|\sin\gamma \quad (29)$$

A more complicated way to represent the stator flux and rotor flux is given as

$$\bar{\Psi}_s = L_s\bar{I}_s + L_m\bar{I}_r \quad (30)$$

$$\bar{\Psi}_r = L_r\bar{I}_r + L_m\bar{I}_s \quad (31)$$

When the projected stator flux value and torque value are compared to the values provided by a command, the error is managed by the hysteresis band controller.

$$H_\Psi = 1 \text{ for } E_\Psi > +HB_\Psi \quad (32)$$

$$H_\Psi = -1 \text{ for } E_\Psi < -HB_\Psi \quad (33)$$

Here, the hysteresis bandwidth of the flux controller is 2HB, and it rotates anticlockwise. The torque control loop has three digital output levels that are connected in this way:

$$H_{\text{te}} = 1 \text{ for } E_{\text{te}} > +HB_{\text{te}} \quad (34)$$

$$H_{\text{te}} = -1 \text{ for } E_{\text{te}} < -HB_{\text{te}} \quad (35)$$

$$H_{\text{te}} = 0 \text{ for } -HB_{\text{te}} < E_{\text{tc}} < +HB_{\text{te}} \quad (36)$$

3 A Nonlinear Model - Predicting Approach to Achieving Optimal Direct Torque Control in PMS Motors

3.1 PMSM Mathematical Model

When planning a nonlinear model predictive control strategy, it is necessary to first think about the features of the EV system. Modeling the dynamic behaviour of a PMSM in the form of a (d, q) rotor that revolves around the frame of reference yields the following nonlinear affine form:

$$x(t) = Ax(t) + Bu(t) + B_d\Lambda_d\ (t) \quad (37)$$

Where

$$A = \begin{bmatrix} -\frac{R_s}{L_d} & \frac{L_q}{L_d}W \\ -\frac{L_q}{L_d}W & -\frac{R_s}{L_q} \end{bmatrix} \quad (38)$$

$$B = \begin{bmatrix} \frac{1}{L_d} & 0 \\ 0 & \frac{1}{L_q} \end{bmatrix} \quad (39)$$

$$B_d = \begin{bmatrix} 0 \\ 1 \end{bmatrix} \quad (40)$$

The conventional wisdom holds that an MPC method discretizes the decision-making approach since T stands for both the input vectors and the state variables in constant time. For each time instant k+1, the projected state is given by an approximation of first order derived from Euler's formula.

$$x_m(k+1) = A_m x_m(k) + B_m u_m(k) + B_{dm\wedge_m}(k) \quad (41)$$

Where

$$A_m = \begin{bmatrix} 1 - \frac{R_s}{L_d}t_s & \frac{L_q}{L_d}wt_s \\ -\frac{L_q}{L_d}wt_s & 1 - \frac{R_s}{L_q}t_s \end{bmatrix} \quad (42)$$

$$B_m = \begin{bmatrix} \frac{1}{L_d}t_s & 0 \\ 0 & \frac{1}{L_q}t_s \end{bmatrix} \quad (43)$$

$$B_{dm} = \begin{bmatrix} 0 \\ t_s \end{bmatrix} \quad (44)$$

where, $xm(k)$ and $xm(k$+1) represent (k and k+1) time state variables, respectively while $um(k)$ and $um(k-1)$ represent the input control vectors for the k and k+1 processing time respectively. $u_m(k) = u_m(k-1) + \Delta u_m(k)$ (45)

The restricted stator current um (k) is used to construct a stator current vector d-q, whereas id(k) and iq(k) are calculated from um (k) using Park's modification.

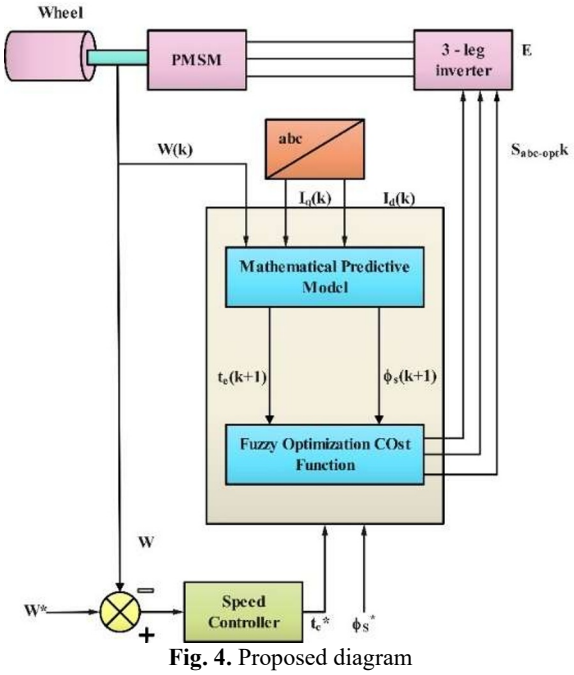

Fig. 4. Proposed diagram

The in-wheel motor with NMP-DTC, PMS system is depicted in Figure 4 in a schematic form. Inventions that use anti-windup devices are a technological controller's speed. The dq stator current materials, a key factor for stator flux and electromagnetic torque forecasting, can be predicted. They also detail the three-phase inverters' estimated switching states. The rotor position angle (k) is attained from an encoder, and the

rotor speed over a sample period can be evaluated using Euler's approximation technique.

$$w(k) = \frac{\theta(k)-\theta(k-1)}{t_s} \quad (46)$$

The following is done to construct the stator flux linkage using the anticipated d−q stator current components (3):

$$\phi_d(k+1) = L_d i_d(k+1) + \phi_f \quad (47)$$

$$\Phi_q(k+1) = L_q i_q(k+1) \quad (48)$$

The magnitude is given by

$$\phi_s(k+1) = \sqrt{[\phi_d(k+1)]^2 + \left[\phi_q(k+1)\right]^2} \quad (49)$$

$$t_e = \frac{3}{2}\left[\frac{P}{2}\right]\frac{L_m}{LL'}|\Psi_r||\Psi_s|\sin\gamma \quad (50)$$

The complex form of the stator flux and rotor flux is given by

$$\bar{\Psi}_s = L_s\bar{I}_s + L_m\bar{I}_r \quad (51)$$

$$\bar{\Psi}_r = L_r\bar{I}_r + L_m\bar{I}_s \quad (52)$$

On further comparing the command stator flux and torque data with the estimated values of stator flux and torque, the error is detected using a hysteresis band processor.

$$H_\Psi = 1 \text{ for } E_\Psi > +HB_\Psi \quad (53)$$

$$H_\Psi = -1 \text{ for } E_\Psi < -HB_\Psi \quad (54)$$

In this scenario, the flux actuator's hysteresis frequency will be 2HBΨ, which is rotating counterclockwise. The torque control loop's various digital output levels are connected as follows:

$$H_{\text{te}} = 1 \text{ for } E_{\text{te}} > +HB_{\text{te}} \quad (55)$$

$$H_{\text{te}} = -1 \text{ for } E_{\text{te}} < -HB_{\text{te}} \quad (56)$$

$$H_{\text{tc}} = 0 \text{ for } -HB_{\text{tc}} < E_{\text{tc}} < +HB_{\text{te}} \quad (57)$$

3.2 IFODPSO-Fuzzy Logic Controllers-Based Direct Torque Control

The IFODPSO-FLC is a hybrid methodology that combines FLCs with fractional order Darwinian particle swarm optimization (FODPSO). Figure 4 shows the Direct torque control structure that is based on IFODPSO-FLC. Using the IFODPSO optimization method, the controller is provided with the determined error.

4 Simulation Results

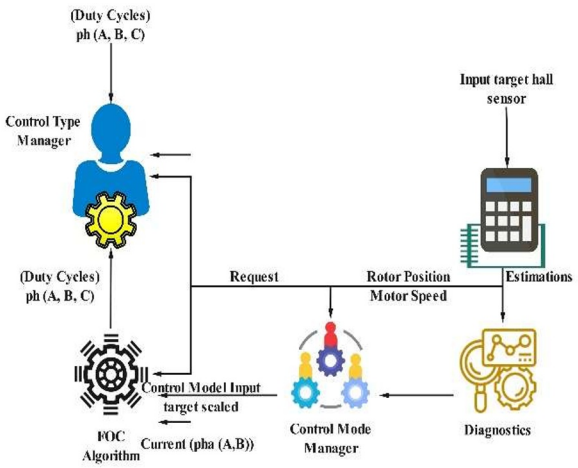

Fig. 5. A DTC system based on IFODPSO-FLC

Displaying the maximum amount of wind energy while decreasing the amount of error and consumption in mechanical power formation by turbines is of the utmost importance. Figure 6 displays the flow diagram of the method, and Figure 5 shows the IFODPSO technique, that is according to the PSO algorithm. To get the required minimum and maximum values, it is optimized using a potential IFODPSO technique. In principle, computer algorithms such as particle swarm optimization (PSO) can make a problem easy to solve by trying many possible solutions until one works. In the Particle Swarm Optimization (PSO) algorithm, "particles" stand in for potential solutions, and they start searching the search space for the best one. Particle swarm optimization (PSO) generates a congested search space by calculating particles near the undesirable solution.

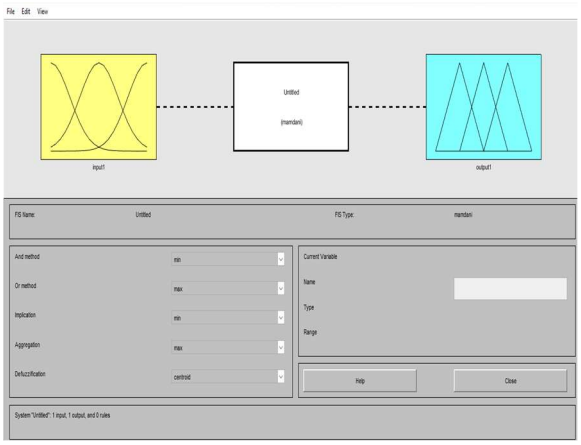

Fig. 6. An optimization-based fuzzy system

Consequently, a method called Darwinian PSO was employed to ascertain the solution to the issue. When compared to the PSO, the DPSO's use of numerous parallel PSO techniques—in which all swarms operate independently is striking. On the other hand: if the search returns unsatisfactory results, it is just stopped and a new area is searched. This causes Darwinian PSO to become stuck, which in turn shortens the lifetimes of swimming particles and causes them to be automatically removed from the search region. Because of this, reaching the point of convergence is a very time-consuming method. To handle both the complexity of DPSO and the need to manage its convergence rate, it was proposed that DPSO could be utilized as a strategy. Figure 7 shows the DPSO, which suggests fractional ordering. Dynamic events and particle trajectories benefit from this fractional order because it demands an endless number of constraints to be fulfilled.

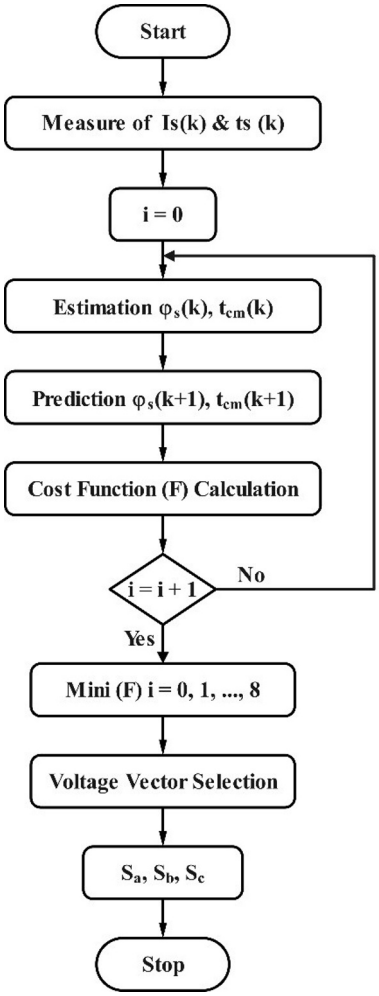

Fig. 7. Fuzzy logic-based IFODPSO flowchart

A vehicle dynamics simulation model is presented here to evaluate the efficacy of an ASR/ABS longitudinal control system in testing the acceleration and deceleration capabilities of 4WID EVs under different road conditions. The four in-wheel motors, which have two inverters powered by a DC voltage source, are managed by a novel master control system that employs nonlinear model prediction for direct torque control. Starting with a speed of 0 m/s, the car model will accelerate to 21 m/s. With this mode of acceleration, the adhesion between the wheels decreases for 5s following the initial loss at 7s. Motor torques, traction forces, compensation, driver positions, vehicle and wheel speeds, angular accelerations (both threshold and real), slip ratios, and model results were summarized. The motor or electrical machine parameters like Ld and Rs, describe its unique electrical characteristics. The direct-axis inductance, abbreviated as Ld, is the measurement of the response of the magnetic field in motor to variations in the DC axis. The electrical resistance that the current passing by the motor's stator windings encounters is known as the stator resistance (Rs).

4.1 Analysis of Comparison

Table 2. An analysis of various optimization techniques

Optimization strategies	Function of Fitness	Time to rise	Scalability of algorithms	Loss of switching
DTC-existed	High	High	Simple	High
DTC-BOA	Moderate	Medium	Good	High
FOC-GA	Moderate	Medium	Complex	Medium
FOC-Fuzzy	L	L	MC	L
IFODPSO-Fuzzy Logic Controller (Proposed)	L	VL	Good	L

(low – L, very low -VL, more complex – MC)

The electric speed was tested on different surfaces, as shown in Table 2. All four wheels experience a quick increase in longitudinal slip as the vehicle speeds up toward a uneven road. The slip ratio stays below the ideal range of 0.05 for each wheel. The results demonstrated that the ASR control can keep the slip ratios close to their ideal values, which makes the electric vehicle more stable. The real slip ratios can follow their ideal slip ratios under various road conditions.

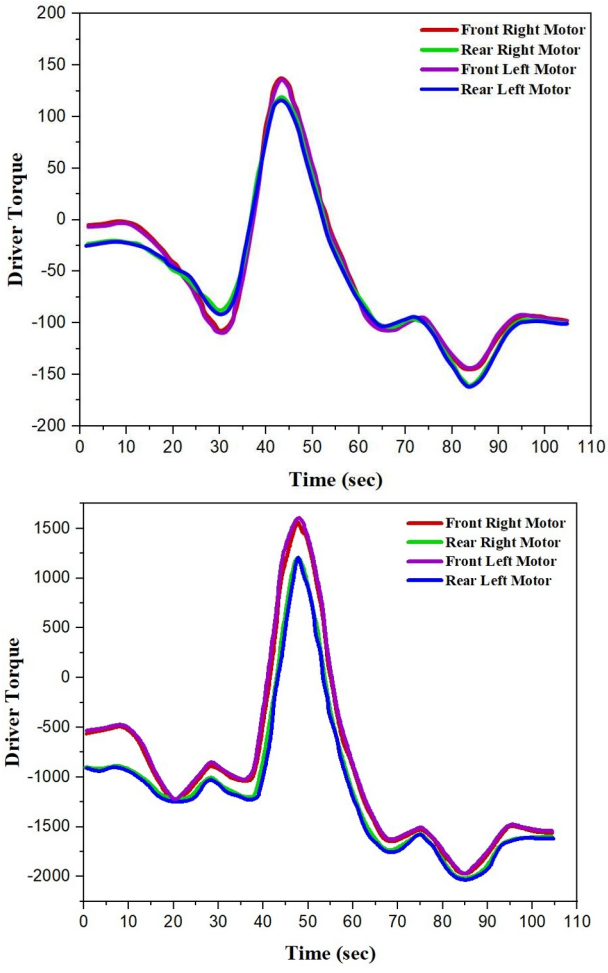

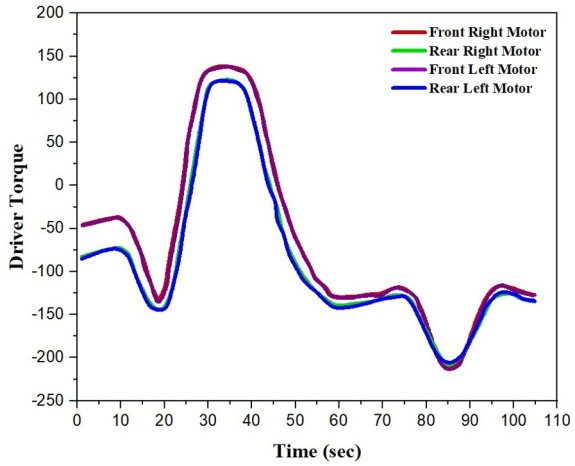
Front Right Motor
Rear Right Motor
Front Left Motor
Rear Left Motor
Driver Torque
Time (sec)

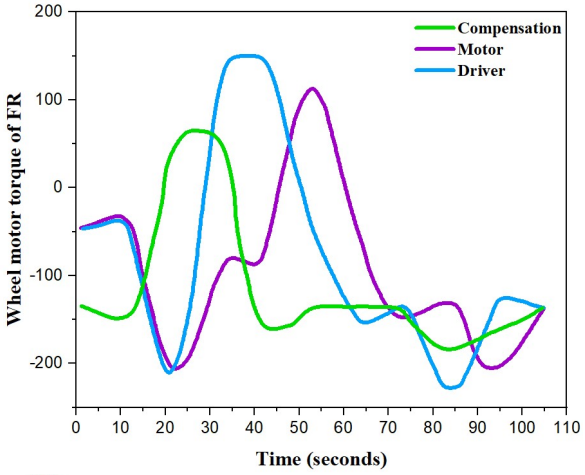
Compensation
Motor
Driver
Wheel motor torque of FR
Time (seconds)

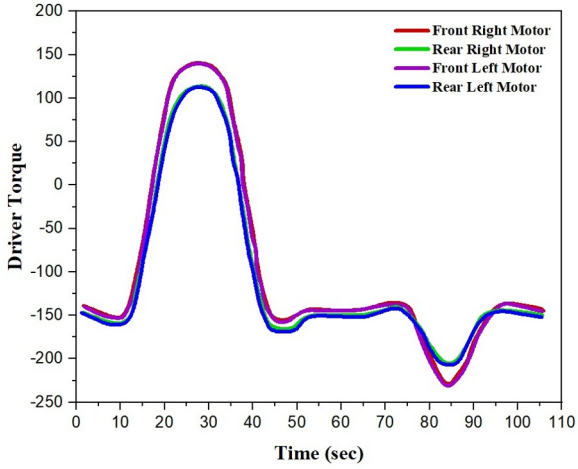
Front Right Motor
Rear Right Motor
Front Left Motor
Rear Left Motor
Driver Torque
Time (sec)

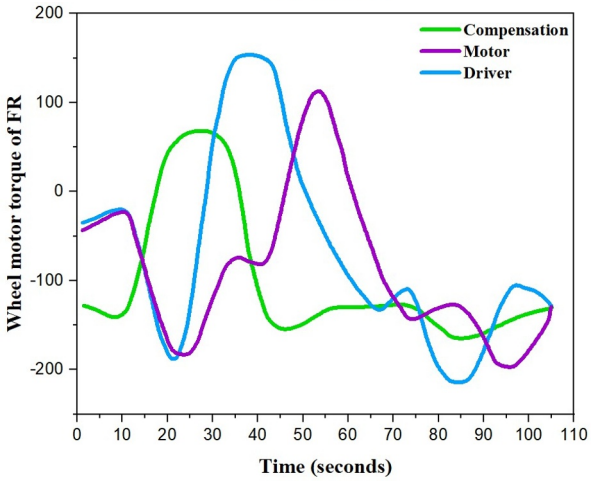
Compensation
Motor
Driver
Wheel motor torque of FR
Time (seconds)

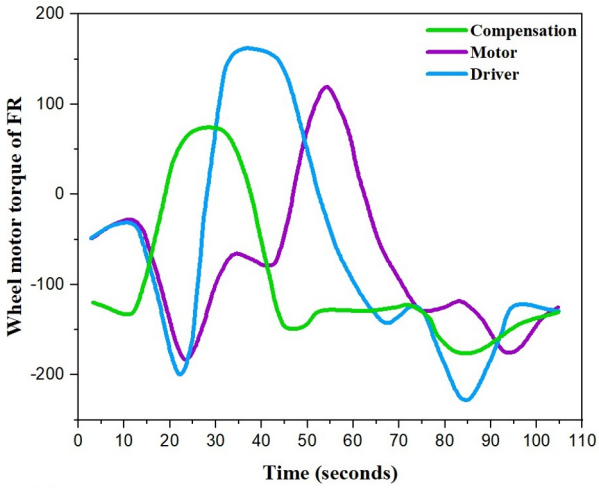
Compensation
Motor
Driver
Wheel motor torque of FR
Time (seconds)

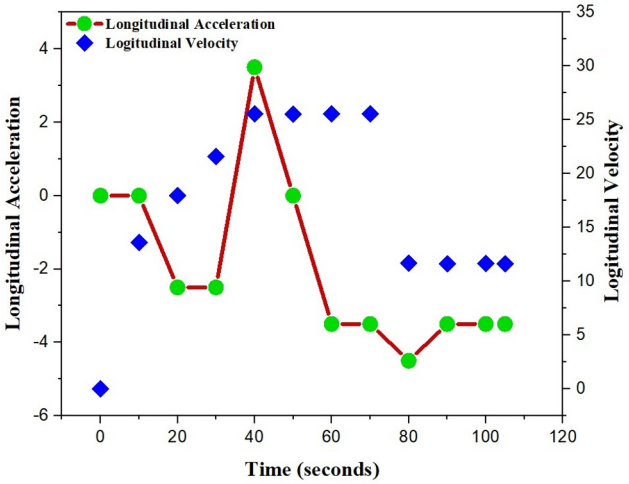
Longitudinal Acceleration
Logitudinal Velocity
Longitudinal Acceleration
Logitudinal Velocity
Time (seconds)

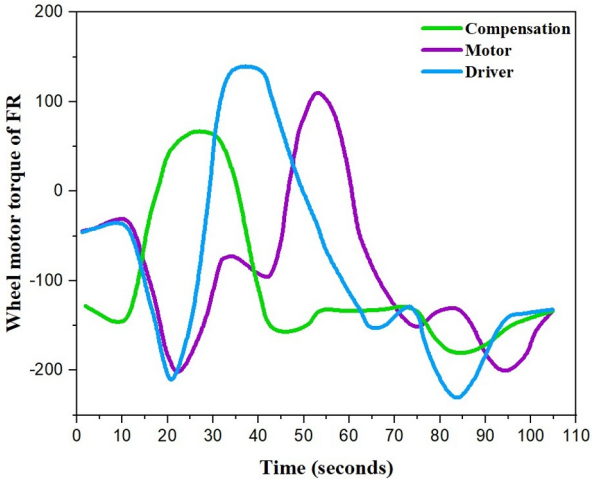
Compensation
Motor
Driver
Wheel motor torque of FR
Time (seconds)

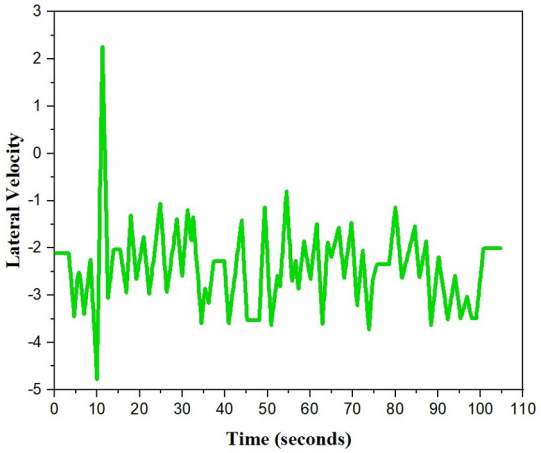
Lateral Velocity
Time (seconds)

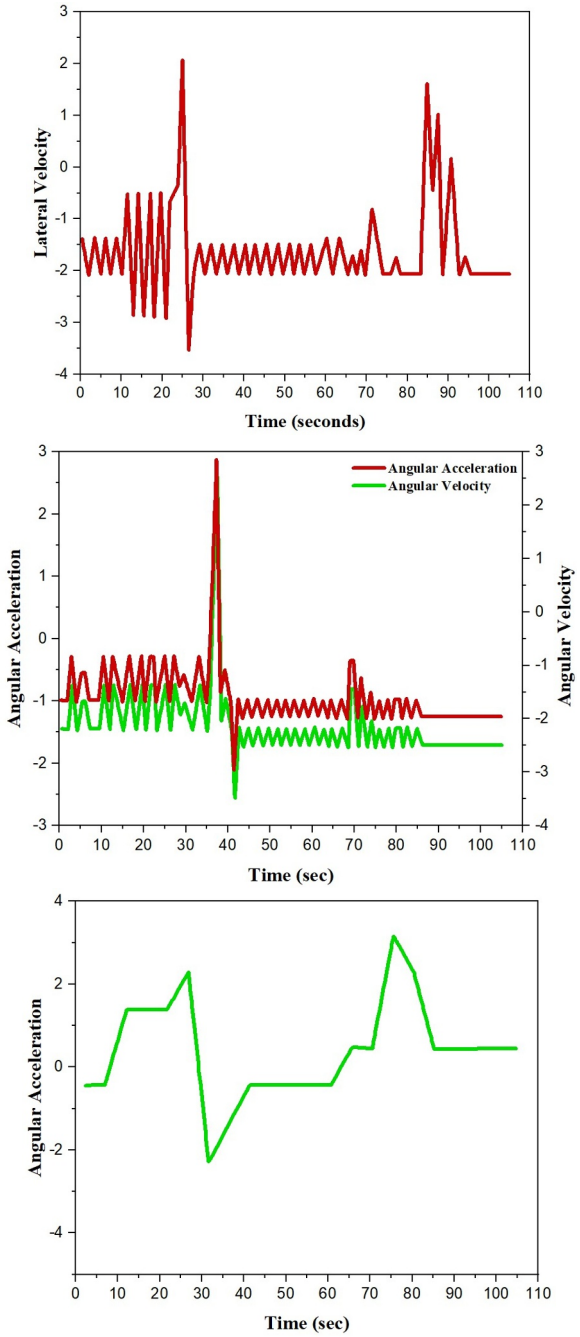

Fig. 8. Analyze the results of the EV simulation

Even when acceleration slip regulation is no longer adhered, ASR significantly affects the vehicle's speed and the in-wheel motors speed maintenance capabilities. Consequently, the ASR controller was developed to compensate for the prevention of wheel slip, which led to a considerable reduction in angular acceleration errors (Figure 8(a)). This was done in order to reduce the motors' torque. This would allow the wheels to adhere and prevent the vehicle from slipping. The controller's imposed torques are shown in Figure 8(g), while the motor torques' fluctuations are shown in Figure 8(f). As shown in Figure 8(h), the driving wheels maintain their traction forces even when adhesion is lost. Use the braking manoeuvre. From 21 m/s to 0 m/s should take about 10 s, or 30 seconds, according to expectations for the vehicle model. The fourth wheel experiences a five-second loss of adhesion following 32 seconds of deceleration due to this deceleration style. All four wheels start to exhibit less longitudinal slip after this change. The ABS control has maintained the wheel slip ratios in an ideal range, as shown in Figures 8(i)-8(3), guaranteeing a smooth representation of the wheel slip ratios. When considering the braking effectiveness of an electric vehicle, this might be seen as mainly beneficial. The simulation results show that the suggested NMP-DTC accurately tracks torque and speed, even under the different adherence conditions that the EV traction operates under. The robustness of the longitudinal control is proven by analyzing the simulation results across a wide range of driving scenarios. Finding the optimal longitudinal slip ratio takes very little time by contrasting the wheels' slip ratios; the results are identical to those obtained when accelerating or decelerating.

5 Conclusions

Finally, a stator resistance device that compensates using PI fuzzy logic is integrated into the suggested sensor-less FL DTC system for in-wheel EVs. This device effectively reduces the effect of variations in stator resistance. The IFODPSO-FLC method achieves precise torque control with a high success rate by integrating FLC with Darwinian PSO of fractional order techniques. The first step of the process is to find the torque inaccuracy by examining the torque rotor and torque connection. The IFODPSO-FLC technique enhances control performance by feeding the calculated error back to the controller. Extensive MATLAB-Simulink simulations were conducted to ascertain the most effective simulation model for every system. The results show that the method was well-designed to achieve accurate torque control and minimize torque errors. The overall performance of in-wheel electric vehicles can be improved by combining the sensor less fuzzy DTC, PI-fuzzy stator resistance compensator, and IFODPSO-FLC technique.

References

1. P. Ponce, B. MacCleery, L. A. Soriano, M. García, V. Leví, A. Molina, Expanding electric vehicles lifetime in power electronic stage using an optimized fuzzy logic controller. International Journal on Interactive Design and Manufacturing. **16,** (2022).
2. H. Salahuddin, K. Imdad, M. U. Chaudhry, D. Nazarenko, V. Bolshev, M. Yasir, Induction Machine-Based EV Vector Control Model Using Mamdani Fuzzy Logic Controller. Applied Sciences (Switzerland). **12,** (2022).
3. V. Jesus Bobin, M. Marsaline Beno, Performance Analysis of Optimization Based FOC and DTC Methods for Three Phase Induction Motor. Intelligent Automation and Soft Computing. **35,** (2023).
4. Jasmine Gnana Malar, C. Agees Kumar, A. Gnana Saravanan, Iot based sustainable wind green energy

for smart cites using fuzzy logic based fractional order Darwinian particle swarm optimization. Measurement (Lond). **166,** (2020).
5. V. Koneti, G. Vulasala, Performance analysis of brush less DC motor drive using fractional order controller with PSO algorithm. Recent Advances in Electrical and Electronic Engineering **12,** (2019).
6. M. S. Couceiro, J. A. Tenreiro MacHado, R. P. Rocha, N. M. F. Ferreira, A fuzzified systematic adjustment of the robotic Darwinian PSO. Rob Auton Syst. **60,** (2012).
7. J. Ratchanyaraj, R. S. Ravindran, Developed an Improved Fractional Ordered Darwinian Particle Swarm Optimization Using Fuzzy Logic Controller to Improve the Performance Measures on E-Vehicle. Electric Power Components and Systems. (2023).
8. S. Gupta, P. K. Biswas, S. Debnath, J. Laldingliana, Optimization Techniques Used in Active Magnetic Bearing System for Electric Vehicles. in Artificial Intelligent Techniques for Electric and Hybrid Electric Vehicles. (2020).
9. J. Wang, S. Gao, K. Wang, Y. Wang, Q. Wang, Wheel torque distribution optimization of four-wheel independent-drive electric vehicle for energy efficient driving. Control Eng Pract. **110,** (2021).
10. M. Vairavel, R. Girimurugan, C. Shilaja, G.B. Loganathan, J. Kumaresan, Modeling, validation and simulation of electric vehicles using MATLAB. In AIP Conference Proceedings. 2452, (2022).
11. Oubelaid, F. Albalawi, T. Rekioua, S. S. M. Ghoneim, N. Taib, S. A. M. Abdelwahab, Intelligent Torque Allocation Based Coordinated Switching Strategy for Comfort Enhancement of Hybrid Electric Vehicles. IEEE Access. **10,** (2022).
12. S. M. Raafat, R. Hussein, Multivariable Extremum Seeking Control for Power Maximization and PI Tuning of Wind Turbine System, in Third Scientific Conference of Electrical Engineering, SCEE, (2018).
13. M.-S. Wang, M.-F. Hsieh, I. N. Syamsiana, W.-C. Fang, Fuzzy maximum torque per ampere and maximum torque per voltage control of interior permanent magnet synchronous motor drive, Sensors and Materials, **29,** (2017).
14. M. Vairavel, R. Girimurugan, C. Shilaja, C., G.B. Loganathan, G.B. Z. Polat, Analysis of hybrid electrical vehicles: Types, formulation and needs. In AIP Conference Proceedings. 2452, (2022).
15. S. Krim, S. Gdaim, A. Mtibaa, M. F. Mimouni, Control with high performances-based DTC strategy: FPGA implementation and experimental validation. EPE Journal (European Power Electronics and Drives Journal). **29,** (2019).
16. K. Adithya and R. Girimurugan, Benefits of IoT in automated systems, Integration of Mechanical and Manufacturing Engineering with IoT: A Digital Transformation, (Scrivener Wiley, USA, 2023).
17. M. A. A. Jubokawa, R. T. F. Ah King, Efficiency optimization of three-phase induction motor using swarm intelligence. in Climate Change Management. (2013).
18. Y.-C. Luo, C.-L. Tsai, Y.-P. Kuo, Speed estimation of stator field orientation control induction motor drive based on the particle swarm optimization algorithm. Sensors and Materials. **30,** (2018).
19. V. J Neelagandan and V. Sivachadambaranathan, A Comparative Study on the Performance of the Induction Motor with Fuzzy-Based Power Converters. Electric Power Components and Systems. (2023).
20. S. Hesari, A. Hoseini, A new approach to improve induction motor performance in light-load conditions. Journal of Electrical Engineering and Technology. **12,** (2017).
21. N.M. Thomas, S.A. Jerome, Eisoc with ifodpso and dcnn classifier for diabetic retinopathy recognition system. Multimedia Tools and Applications. (2023).
22. F. Kulić, D. Matić, B. Dumnić, V. Vasić, Optimal fuzzy controller tuned by TV-PSO for induction motor speed control. Advances in Electrical and Computer Engineering. **11,** (2011).
23. Ammar, Performance improvement of direct torque control for induction motor drive via fuzzy logic-feedback linearization: Simulation and experimental assessment. COMPEL - The International Journal for Computation and Mathematics in Electrical and Electronic Engineering. **38,** (2019).
24. J. Yu, Z. Zhao, A. Zhao, F. Wang, S. Chen, Improved FODPSO algorithm for load distribution of parallel chillers. Zhongnan Daxue Xuebao (Ziran Kexue Ban)/Journal of Central South University (Science and Technology) **52,** (2021).
25. R. Chakraborty, G. Verma, S. Namasudra, IFODPSO-based multi-level image segmentation scheme aided with Masi entropy. J Ambient Intell Humaniz Comput, **12,** (2021).
26. G. Boukhalfa, S. Belkacem, A. Chikhi, S. Benaggoune, Direct torque control of dual star induction motor using a fuzzy-PSO hybrid approach. Applied Computing and Informatics. **18,** (2022).
27. S. Tripathi, A. Shrivastava, K. C. Jana, Chimp optimization-based fuzzy controller for hybrid electric vehicle speed control using electronic throttle plate. Optim Control Appl Methods. **45,** (2024).